Results of a Strong Interaction, Wake-Like Model of Supersonic Separated and Reattaching Turbulent Flows

LOUIS G. HUNTER JR.* AND BARRY L. REEVES†
Avco Systems Division, Wilmington, Mass.

Results of an interaction theory for supersonic separated and reattaching turbulent boundary layers are presented and compared with recent experiments for flow past a compression ramp. Effects of ramp angle, Mach number, Reynolds number, and upstream pressure gradient are considered for situations where the critical point is located upstream of the trailing edge. When the critical point falls downstream of the trailing edge the whole region of separated flow is influenced by ramp length. In these "short ramp" flows the peak ramp pressure attains a maximum at a critical ramp angle and then decreases with increasing angle. It is shown that this effect is responsible for the spanwise pressure distributions measured by Whitehead and Keyes for flow over a delta wing with a trailing edge flap. Results are also presented for a turbulent boundary layer-shock wave interaction.

Nomenclature

a = sonic velocity
a_r = area of recirculation region
b = half span of delta wing
c_p = specific heat at constant pressure
D = dissipation integral
= function defined by Eq. (9)
G = Clauser equilibrium parameter
H = velocity profile parameter, θ_i/δ_i^* (inverse of usual parameter)
H^* = H at critical point
H_e = stagnation enthalpy of freestream
J = θ_i^*/δ_i^*
K_θ = inverse turbulent Reynolds number
L = length of flat plate
L_f = length of ramp
L_{cr} = distance from corner to critical point
L_s = separation length ahead of corner
M = Mach number
M_∞' = Mach number of inviscid stream after turn to wedge angle α
m = $[(\gamma - 1)/2]M^2$
n = power-law exponent in transformed coordinates
p = static mpressure
$\bar{R}$ = integral defined by Eq. (8)
$Re_{\infty,x}$ = Reynolds number
$Re_{\delta_i^*}$ = Reynolds number based on transformed properties, $U_e\delta_i^*/\nu$
Re/m = Reynolds number per meter
S = ramp span
T_0 = stagnation temperature
u,v = x,y velocity components
U = transformed velocity
y' = distance from centerline of wing
x,y = coordinates parallel and normal to surface
X,Y = transformed coordinates
Z = $(1/\delta_i^*)\int_0^{\delta_i}(U/U_e)dY$
α = wedge angle
α' = angle of attack
β = $(\delta^*/\tau_w)(dp/dx)$
δ = boundary-layer thickness
δ_0' = effective thickness for finite span
$\bar{\delta}$ = δ/δ_0
δ_i^* = $\int_0^{\delta_i}(1 - U/U_e)dY$
$\bar{\delta}_i^*$ = δ_i^*/δ_0
ϵ_i = eddy viscosity in transformed coordinates
$(\epsilon_m)_i$ = maximum eddy viscosity
θ_i = $\int_0^{\delta_i} U/U_e(1 - U/U_e)dY$
θ_i^* = $\int_0^{\delta_i} U/U_e(1 - U^2/U_e^2)dY$
θ_c = half angle of cone
Θ = $\tan^{-1}(v_e/u_e)$
ν = Prandtl-Meyer angle
ρ = gas density
τ = shear stress

Subscripts

c = corner
e = local inviscid
i = transformed
s = separation point
w = wall
cr = critical point
x = along surface
∞ = freestream
0 = upstream of interaction, also
1 = upstream of supercritical jump

Presented as Paper 71-128 at the AIAA 9th Aerospace Sciences Meeting, New York, January 25-27, 1971; received May 19, 1970; revision received November 19, 1970.

* Staff Scientist; now Assistant Professor, Matlow State College, Tullahoma, Tenn. Member AIAA.
† Senior Consulting Scientist.

I. Introduction

DESPITE the fact that there still is no rational nor generally reliable model for calculating the turbulent stress distribution in a compressible turbulent boundary layer, some success has been achieved recently in predicting certain turbulent boundary-layer inviscid flow interactions. These advances in the development of a theoretical approach have been made principally for those flows in which the inner wall layer either disappears or is unimportant in most of the region of interaction. In this situation the problem "reduces" to the analysis of a free shear layer or wake-like flow in a self-induced pressure gradient. Although important questions still remain concerning the general behavior of the turbulent stress in wake-like flows with strong pressure gradient and the flow conditions for which lateral pressure gradients in localized regions of the interaction are important, analyses of the turbulent near wake,[1,2] boundary layers with large blowing[3-5] along a surface and turbulent separated and reattaching flows over compression corners[6] using a strong interaction, wake-like model of the flow have produced results which compare favorably with experiments. Of course, in all these problems the inviscid pressure distribution cannot be prescribed in advance but must be computed locally in response to the growth of the inner dissipative layer.[7]

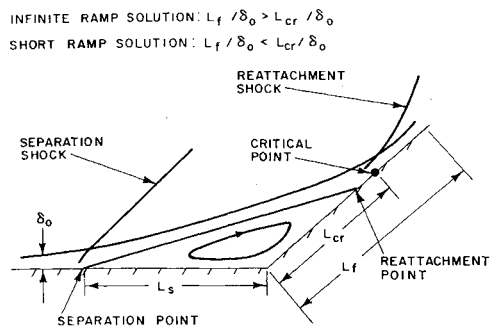

Fig. 1 Schematic representation of turbulent separated and reattaching flow.

The present study is an attempt to apply the turbulent interaction model for separated and reattaching flows developed in Ref. 6 to several important problems associated with control surfaces (flaps) on high-speed aircraft and maneuvering re-entry vehicles. It will be shown that only slight modification of the basic two-dimensional theory leads to reliable calculations of the separated flowfield for practical control configurations, which, up to now, have been analyzed using correlations of experimental data.[8] In fact, by abandoning the incompressible equilibrium flat plate velocity profiles and introducing more general initial conditions for the boundary layer upstream of separation, length scales of the separated flow and pressure distributions obtained in cold wall experiments[6] are shown to be in good agreement with the present adiabatic theory. This is accomplished by using the cold wall value of δ_0 as the proper reference length scale of the interaction.[6] The analysis can also be applied to boundary layers in pressure gradients upstream of separation.

The strong interaction-moment integral method for turbulent separated and reattaching flows is reviewed briefly in Sec. II. Included in this section is the revised treatment of initial conditions upstream of separation. In Sec. III the effect of ramp length on the extent of separation and rate of pressure recovery is examined. Two types of solutions are distinguished. The first, which we identify as an "infinite ramp solution," is one in which the critical point (throat) is located upstream of the ramp trailing edge (Fig. 1). Since in this case the reattached boundary layer is supercritical at the trailing edge, there is no upstream influence produced by the sudden expansion. Thus, the separated flow region is independent of ramp length even though the degree of pressure recovery downstream of the critical point can quite obviously depend on ramp length. In the second, "short ramp solution," the critical point computed on the basis of infinite ramp boundary conditions would fall downstream of the ramp trailing edge. In this situation the whole region of separated flow is affected because, even though the flow may have reattached, the subcritical boundary layer expansion at the trailing edge is communicated upstream.

Results for both infinite and short ramps are compared with several sets of two-dimensional experimental data in Sec. IV.

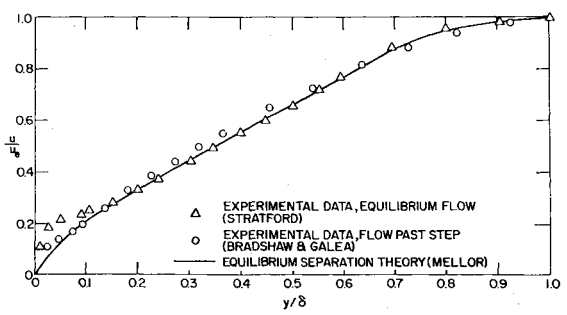

Fig. 2 Low-speed turbulent separation profiles.

By using a strip method for flow over a delta wing with a trailing edge ramp, it is shown that important spanwise changes in pressure are the result of the shift in location of the critical point along the span. Finally, a semiempirical correlation of effects of finite span is proposed in Sec. V as a correction of the present two-dimensional theory. The theory together with the finite span correction is used to calculate pressure distributions on a blunted cone with trailing edge flap at 0° and 7° angle of attack.

II. Review of the Strong Interaction Moment Integral Method for Turbulent Separated and Reattaching Flows

Flow Model and Interaction Equations

In virtually all supersonic turbulent reattaching flows there is a subcritical-supercritical transition, either at the critical point on "infinite" ramps or at the trailing edge singular point on short ramps.[6] Because the flow downstream of this transition is unable to communicate with and influence the flow upstream, details of the supercritical portion of the flow after reattachment can be ignored in the analysis of separated and reattaching flow interactions. Moreover, in most high-speed turbulent interactions separation occurs over a very short streamwise distance of only two boundary-layer thicknesses or less.[9] Consequently, the jump from a supercritical flow upstream to a subcritical flow, which initiates an interaction, can be approximated quite well by a jump to separation.[6,10] In seeking a solution of turbulent separated and reattaching flows with the moment integral method we need only be concerned with the interaction region between the separation point and critical point (or trailing edge for short ramps). In this region it is assumed, following some observations made by Seddon[11] in experiments on turbulent boundary layer-shock wave interactions, that the flow has a wake-like character,‡ so that: 1) the wall layer (and wall stress) is assumed unimportant, and 2) the velocity and stress profiles are assumed to be wake-like and are treated as essentially laminar profiles with the viscosity given by a prescribed variation of the eddy viscosity (as a function of y). The profiles, or actually the profile integral functions are then properly normalized and matched with an equilibrium turbulent layer at separation measured by Stratford.[15] Assumption 2 was proposed and used by Clauser[13,14] to calculate the wake-like outer layer of equilibrium incompressible layers.

If the wall stress is negligible compared with the maximum turbulent stress in the layer in the region between the separation point and critical point, the integral equations of continuity, momentum and first velocity moment become, respectively, for adiabatic flow and $\partial p/\partial y = 0$ (Ref 6).

$$\left[H + \left(\frac{1+m_e}{m_e}\right)\right]\frac{d\delta_i^*}{dX} + \delta_i^*\frac{dH}{dX} + f\frac{\delta_i^*}{M_e}\frac{dM_e}{dX} = \frac{\tan\Theta}{m_e} \quad (1)$$

$$H\frac{d\delta_i^*}{dX} + \delta_i^*\frac{dH}{dX} + (2H+1)\frac{\delta_i^*}{M_e}\frac{dM_e}{dX} \simeq 0 \quad (2)$$

$$J\frac{d\delta_i^*}{dX} + \delta_i^*\frac{dJ}{dX} + \frac{3J\delta_i^*}{M_e}\frac{dM_e}{dX} = D \quad (3)$$

where[2]

$$dY = \frac{a_e\rho}{a_\infty\rho_\infty}dy \qquad dX = \frac{a_e\rho_e}{a_\infty\rho_\infty}dx \quad (4)$$

$$D = \frac{2}{U_e^3}\int_0^{\delta_i}\bar{\epsilon}(\partial U/\partial Y)^2 dY \quad (5)$$

‡ Using the law of the wall-law of the wake representation, Coles[12] also showed that the dominant wake component at a point of separation or reattachment produces a boundary layer which is locally a "pure wake flow."

or

$$D = K_\theta H \bar{R} = 2\int_0^{\delta_i} \frac{\tau_i}{\rho U_e^2} \frac{\partial (U/U_e)}{\partial Y}\, dY \tag{6}$$

and where

$$\bar{\epsilon} = (\rho_r/\rho_e)^2 K_\theta U_e \theta_i (\epsilon/\epsilon_m)_i \quad (\rho_r \approx \rho_e) \tag{7}$$

$$\bar{R} \equiv \frac{2\delta_i^*}{U_e^2}\int_0^{\delta_i} \left(\frac{\epsilon}{\epsilon_m}\right)_i \left(\frac{\partial U}{\partial Y}\right)^2 dY \tag{8}$$

and

$$= \frac{3\gamma - 1}{\gamma - 1} + \left[2 + \frac{\gamma + 1}{\gamma - 1}\left(\frac{m_e}{1 + m_e}\right)\right] H + \left[\frac{M_e^2 - 1}{m_e(1 + m_e)}\right] Z \tag{9}$$

From Eq. (7), K_θ is an inverse turbulent Reynolds number, which, for equilibrium flows, was shown[6] to vary between 0.027 for zero pressure gradient, attached boundary layers and 0.05 for zero pressure gradient, free shear layers.

Since the strength of the separation shock seldom exceeds a value of 2, even at hypersonic speeds, the outer flow can generally be assumed isentropic, possibly as far downstream as the critical point. Thus, in these solutions the inclination of the inviscid streamlines at the edge of the layer is related to the local edge Mach number by the Prandtl-Meyer relation. Downstream of the critical point, where the inviscid flow entrained by the layer has passed through the strong reattachment shock, a better approximation for the flow angle-pressure relationship is given by the imbedded-Newtonian-plus-centrifugal formula.

Equations (1–3), when properly normalized and solved explicitly for the unknown derivatives, become

$$(\bar{\delta}_i^*/M_e)(dM_e/d\bar{X}) = n_1/d \tag{10}$$

$$\bar{\delta}_i^*(dH/d\bar{X}) = n_2/d \tag{11}$$

$$d\bar{\delta}_i^*/d\bar{X} = [-n_2 - n_1(2H + 1)]/Hd \tag{12}$$

where

$$n_1 = [J - H(dJ/dH)](\tan\Theta/m_e) + (H - B)D \tag{13}$$

$$n_2 = J(H - 1)(\tan\Theta/m_e) + (2H + 1)DB - HDf \tag{14}$$

$$d = [J - H(dJ/dH)]f + (H - 1)J + B[(2H + 1)(dJ/dH) - 3J] \tag{15}$$

$$B = H + (1 + m_e)/m_e$$

$$\bar{\delta}_i^* \equiv \delta_i^*/\delta_0 \qquad \bar{X} \equiv X/\delta_0 \tag{16}$$

$$\Theta = \nu(M_\infty) - \nu(M_e) \tag{17}$$

Contrary to the situation for an attached, supercritical turbulent boundary layer, with an inner wall layer and outer wake layer, it is assumed that velocity profiles in the wake-like separated flow can be approximately represented as a one-parameter family, analogous to laminar flows. This assumption stems from Clauser's[14] treatment of the wake-like outer layer of equilibrium flows in which he showed that if the eddy viscosity is constant or has a self-similar variation across the wake layer, the equilibrium turbulent profile in the wake layer has the same form as a laminar similarity solution.

In Ref. 6 the integral functions H, J, etc., were evaluated for separated flows in the manner prescribed by Clauser for wake-like layers by assuming that the integral profile functions retain the same dependence on H, when properly normalized, as in laminar flow. These functions were then matched with the values obtained from Stratford's experimental equilibrium profile at separation. This profile is virtually identical to the separation profile measured by Bradshaw and Galea[16] in flow past a forward facing step, and is in good agreement with the profile predicted at separation by the equilibrium theory of Mellor and Gibson[17] (Fig. 2). As in the case of laminar strong interactions,[18] the separated profiles were "unhooked" from the corresponding equilibrium pressure gradient parameter. The integrals were then expressed as one-parameter functions of H, i.e., $J = J(H)$, $\bar{R} = \bar{R}(H)$, etc. In this way the turbulent stress profile is determined by the local mean velocity profile, but the latter is found from solution of the integral moment equations at each station, and as a result, depends on upstream history of the flow.

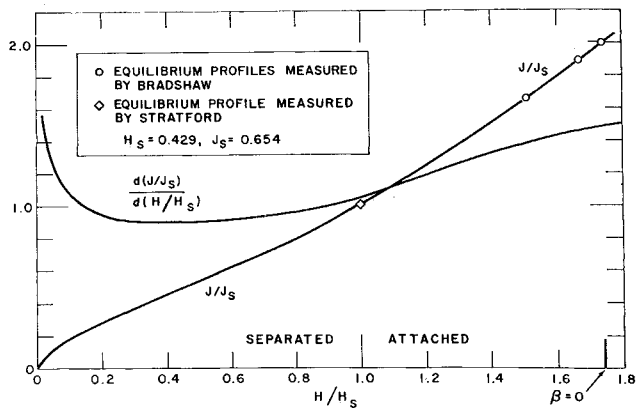

Fig. 3 J and dJ/dH distributions from equilibrium boundary layers.

The integral functions obtained in Reference 6 using the aforementioned procedure are shown in Figs. 3 and 4. Figure 4 also shows the tentative linear "equilibrium" variation of K_θ proposed in Ref. 6. With J, R, Z and K_θ specified as one-parameter families of H in the wake-like region, Eqs. (10–12) are three simultaneous, nonlinear first order equations for M_e, H and $\bar{\delta}_i^*$. Details of the numerical integration and the solution for the location of the critical point were given in Ref. 6. The normalized thickness of the turbulent layer is obtained from Eq. (4)

$$\bar{\delta} = (a_\infty \rho_\infty / a_e \rho_e)[1 + Z + m_e(1 + H)]\bar{\delta}_i^* \tag{18}$$

Revised Initial Conditions Upstream of Separation

As shown by Crocco[10] using the Crocco-Lees theory, and as later verified by Todisco and Reeves[6] using the present moment method, the zero pressure gradient, turbulent boundary layer is supercritical at Mach numbers above about 1.3. It was also shown that above Mach 1.3 a rapid distortion of the layer (supercritical-subcritical "jump") upstream of

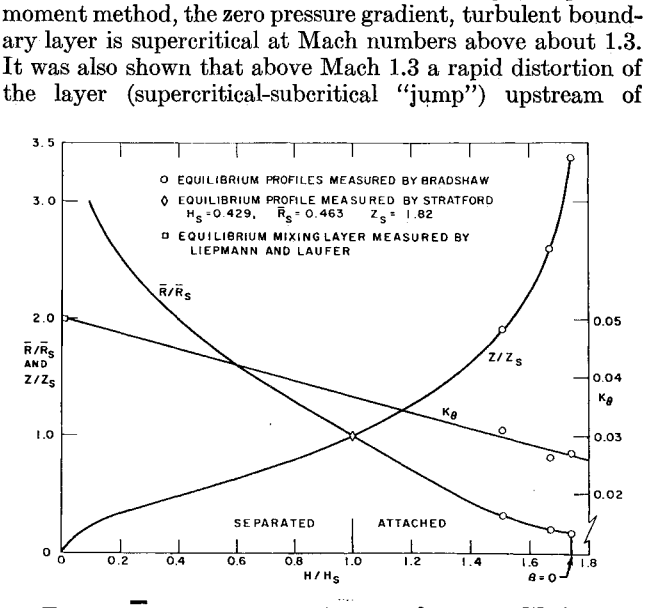

Fig. 4 $\bar{R}$, Z and K_θ distributions from equilibrium boundary layers.

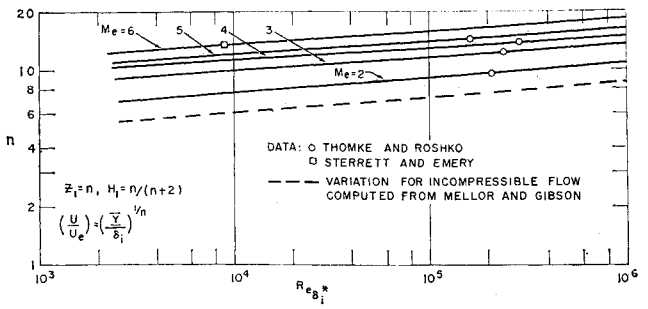

Fig. 5 Variation of velocity profile power-law in transformed coordinates with Reynolds number for flat plate.

separation is required in order for the flow to respond properly as a strong interaction compression. This rapid distortion, which occurs over a length scale much smaller than the length of the over-all interaction, can be described approximately by a set of jump conditions with the downstream boundary conditions of the jump given by the conditions at separation. The jump relations and several solutions were given in Ref. 6, where it was found that the strength of the jump p_e/p_1 generally is about 2. In Ref. 6 the integral functions H_1 and Z_1 required for the upstream conditions of the jump were obtained from the incompressible equilibrium flat plate solutions of Mellor and Gibson.[17] Both integrals are slowly varying functions of $Re_{\delta i^*}$ (see Table 1 of Ref. 6).

In the present study we allow for a more general set of initial conditions for the upstream boundary layer, so that dp/dx need not be zero initially. Moreover, we have abandoned use of the equilibrium incompressible profiles[17] for flows where $dp/dx = 0$ initially. By approximating the upstream boundary layer as a power law in physical coordinates and by matching with the initial momentum thicknesses measured by Thomke and Roshko[19] and Sterrett and Emery,[20] a tentative semiempirical variation of the transformed velocity profile power law with Reynolds number and Mach number is obtained, which extends up to Mach 6 for adiabatic flows. It will be shown that the value of n in the power law obtained from the experimental profiles is a function of Mach number, and can be considerably larger than the value obtained using the compressibility transformation and incompressible equilibrium solutions.

Assuming that the boundary layer thickness δ_0 upstream of separation is known, we wish to find the integral functions H_1 and Z_1 of the transformed velocity profile consistent with a measured momentum thickness just upstream of separation.[19,20] For power law velocity profiles in transformed coordinates

$$(U/U_e)_1 = (Y/\delta_i)^{1/n} \tag{19}$$

the functions H_1 and Z_1 are

$$Z_1 = n; \quad H_1 = n/(n+2) \tag{20}$$

The momentum flux in the layer upstream of the jump at separation is

$$\int_0^\delta \rho u^2 dy = \rho_\infty a_\infty u_{e1} M_{e1} (\delta_i^*)_1 (Z_1 - H_1) \tag{21}$$

Using the Crocco integral to approximate the density distribution across the layer,

$$\frac{\rho_e}{\rho} = (1 + m_e)\left[\frac{H_w}{H_e} + \left(1 - \frac{H_w}{H_e}\right)\frac{u}{u_e}\right] - m_e\left(\frac{u}{u_e}\right)^2$$

the boundary-layer thickness at the beginning of the interaction becomes

$$\delta_0 \equiv \delta_1 = \left[1 + Z_1 + m_{e1}(1 + H) + (1 + m_{e1}) \times \left(\frac{H_w}{H_e} - 1\right)\right]\delta_i^* \tag{22}$$

Assuming that the compressible velocity profile can be written as a power law in physical coordinates, i.e.,

$$\left(\frac{u}{u_e}\right)_1 = \left(\frac{U}{U_e}\right)_1 = \left(\frac{y}{\delta}\right)_1^{1/N} \tag{23}$$

The equation for the momentum flux becomes

$$\frac{n}{\left[n + 2(1 + m_e) + \dfrac{n+2}{n+1}(1 + m_e)\left(\dfrac{H_w}{H_e} - 1\right)\right]} = \int_0^1 g\left(\frac{y}{\delta}\right) d\left(\frac{y}{\delta}\right) \tag{24}$$

where

$$g\left(\frac{y}{\delta}\right) = \frac{(y/\delta)^{2/N}}{(1 + m_e)\left[\dfrac{H_w}{H_e} + \left(1 - \dfrac{H_w}{H_e}\right)\left(\dfrac{y}{\delta}\right)^{1/N}\right] - m_e\left(\dfrac{y}{\delta}\right)^{2/N}}$$

Since, typically $n \gg 1$ the expression for n becomes

$$n = \frac{(1 + m_e)\,[1 + (H_w/H_e)]\int_0^1 g(y/\delta)d(y/\delta)}{1 - \int_0^1 g(y/\delta)d(y/\delta)} \tag{25}$$

If the compressible displacement and momentum thicknesses are known rather than N, a more convenient form of the integral is

$$\int_0^1 g(y/\delta)d(y/\delta) = 1 - \delta^*/\delta - \theta/\delta \tag{26}$$

Finally, a Reynolds number based on the transformed displacement thickness can be found in terms of the actual Reynolds number based on the initial boundary-layer thickness, Re_{δ_0}

$$Re_{\delta_0} = \frac{n+1}{n+2}\left[n + 2(1 + m_e) + \frac{n+2}{n+1}(1 + m_e) \times \left(\frac{H_w}{H_e} - 1\right)\right] Re_{\delta i^*} \tag{27}$$

or, with $n \gg 1$

$$Re_{\delta i^*} = \frac{Re_{\delta_0}}{[n + (1 + m_e)(1 + H_w/H_e)]} \tag{28}$$

Values of N obtained by Thomke and Roshko at $M_e = 2$, 3, 4 and 5, and a value computed from the data of Sterrett and Emery at $M = 6$ are tabulated in Table 1 as a function of M_e and Re_{δ_0}. A mean value of Re_{δ_0} over a small range of values was selected from Thomke and Roshko's data.

These values of Re_{δ_0} and N were used to compute n and $Re_{\delta i^*}$, which are shown in Fig. 5. Evidently, the transformation does not eliminate the dependence of n on Mach number, and previously reported results obtained using values of n from incompressible equilibrium layers (dashed line in Fig. 5) are expected to be in some error, especially at high Mach numbers.[6] The dependence of n on $Re_{\delta i^*}$ is assumed to be the same as the incompressible variation[17] for all Mach numbers. Thus, for given M_e and Re_{δ_0}, Eq. (28) and Fig. 5 are sufficient to determine $Re_{\delta i^*}$ and n. We shall assume, tentatively, that Fig. 5 is applicable for cold walls as well, and that separation distances for nonadiabatic interactions can be scaled by the proper cold-wall value of δ_0.

Table 1 Variation of velocity profile parameter with Reynolds number and Mach number

M_e	2	3	4	5	6
Re_{δ_0}	2.5×10^6	4×10^6	6×10^6	4×10^6	2.5×10^5
N	8.9	10.5	10.7	10	10

III. Short Ramp Solutions

As long as the critical point ($d = 0, n_1 = 0, n_2 = 0$) of the system of Eqs. (10–12) is located upstream of the trailing edge of the ramp, length scales and pressures in the region of separated flow are unaffected by changes in ramp length. Of course, the extent of pressure recovery downstream of the critical point is a function of length if the pressure has not reached its asymptotic value corresponding to the given ramp angle.

When the calculated location of the critical point falls downstream of the trailing edge solutions of the infinite ramp type are invalid and the downstream boundary condition must be altered to account for the rapid expansion at the trailing edge. The reattachment point must adjust to a change in ramp length and this shift in the position of reattachment influences the whole region of separation. In this situation (short ramp solution), reattachment usually occurs near the trailing edge, and the shear layer does not have a chance to turn through the full ramp angle. In fact, we will show that for short ramps with a fixed value of L_f/δ_0, an increase in ramp angle above some critical angle can actually produce a decrease in peak ramp pressure because of the movement of reattachment toward the trailing edge.

For short ramps, it is assumed, following Ko and Kubota's[21] analysis for laminar flows, that the quantities M_e, $\bar{\delta}_i^*$, and H all remain finite in the abrupt expansion at the trailing edge but that the derivatives dM_e/dX, $d\bar{\delta}_i^*/dX$ and dH/dX approach infinity. Instead of n_1, n_2, and d vanishing simultaneously at the critical point, as on an infinite ramp, the ramp angle is determined by requiring that $d = 0$, $n_1 \neq 0$, $n_2 \neq 0$ at the trailing edge. The result of such a calculation is that just before the trailing edge, $d\bar{\delta}_i^*/dX$ is negative whereas dH/dX and dM_e/dX are positive, so that a peak in pressure occurs downstream of reattachment. For infinite ramp solutions dp/dx is still positive at the critical point as the flow continues to turn parallel to the ramp.[6]

The procedure used to obtain short ramp solutions is facilitated by knowledge of the integration path through the critical point. For a given set of flow conditions calculated up to the corner, the reattachment solutions where $d \to 0$ and the n's remain finite correspond to downstream Mach numbers (M_∞') that are less than M_∞' found for the associated infinite ramp. Thus, by decreasing M_∞' from the infinite ramp value in suitable increments, d can be made to vanish along the integral path at points closer to the corner. The family of solutions generated in this manner have L_f/δ_0 and α as parameters for a fixed value of L_s/δ_0.

IV. Numerical Results and Experimental Comparisons

Infinite Ramp Solutions

The variation of the normalized distance from the corner to the critical point with ramp angle is shown in Fig. 6 for selected values of Mach number and profile shape upstream of separation. The minimum value of L_{cr}/δ_0 shown for each curve is the value obtained for the incipient separation ramp angle, which is a function of Mach number and n. As the ramp angle is increased above this value the reattachment point and critical point move downstream toward the trailing edge. As discussed in the previous section, infinite ramp solutions are valid as long as $L_f/\delta_0 > L_{cr}/\delta_0$. For given Mach number and n an increase in ramp angle of 10 degrees above the incipient separation angle is required to move the critical point downstream roughly 20 boundary-layer thicknesses.

The corresponding variation of the normalized separation distance upstream of the corner with ramp angle is shown in Fig. 7. For a given value of α, L_s/δ_0 decreases with increasing Mach number and n. Thus, for separation on a flat plate with fixed upstream Mach number, both δ_0 and L_s increase as the Reynolds number is increased above the minimum Reynolds number required for fully turbulent separation, because of the forward movement of the transition point. This produces a larger value of L_s until the transition point reaches the vicinity of the leading edge. Then, with still further increase in Reynolds Number, δ_0 decreases and n increases producing a *decrease* in the separation length. This predicted dependence of the separation length on Reynolds number has been verified in the experiments by Thomke and Roshko and Todisco and Reeves.

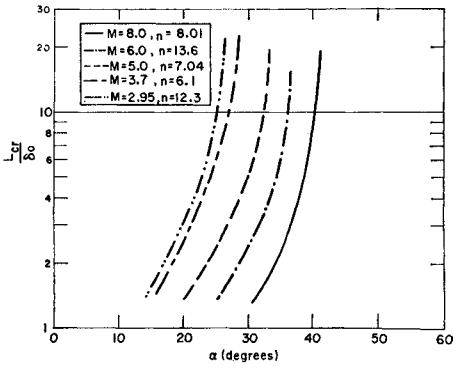

Fig. 6 Nondimensional critical ramp length for various Mach numbers and profile power-laws.

The effect of the profile parameter n on separation length can be seen by comparing the curves at roughly the same upstream Mach number (4.92 and 5). The two curves represent a difference of 10^4 in the value of $Re_{\delta_i^*}$ for separation induced on a flat plate (Fig. 5). Alternatively, these same curves also reflect the change in separation lengths produced by boundary layers in prescribed pressure gradients upstream of separation. Calculations based on recent unpublished data obtained by Lewis[29] at Mach 4 and a Reynolds number based on momentum thickness of about 10^4 showed that the Mach 5 solution for $n = 14.8$ corresponds to a value of β upstream of separation of about -3, whereas the solution for $n = 7$ corresponds to $\beta = 1.5$.

Comparisons of the theory with pressure distributions measured by Thomke and Roshko[16] at $M = 3.93$ and 4.92 are shown in Figs. 8 and 9, respectively. The theory appears to predict quite well the separation distance L_s and the pressure distribution up to the corner. The rate of pressure recovery on the ramp, however, is somewhat more rapid than predicted.

Figure 10 shows a new comparison with the experimental results obtained for a cold wall at Mach 6.5 by Todisco and Reeves[6] using the revised set of initial conditions (Sec. II). In this case the cold wall value of δ_0 was used as the reference length. The results for separation length and pressure distri-

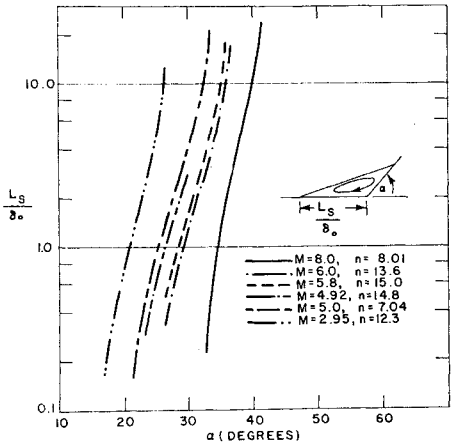

Fig. 7 Nondimensional separation length for various Mach numbers and profile power-laws.

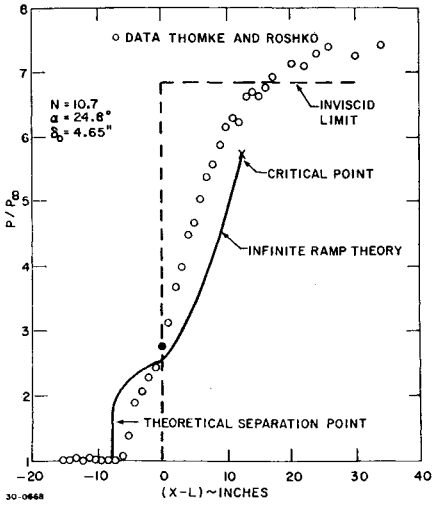

Fig. 8 Comparison of experimental and theoretical pressure distributions, $M = 4$, $Re = 1.2 \times 10^6$/in.

bution upstream of the corner are in better agreement than reported in Ref. 6 but, as in the comparison with Thomke and Roshko's data, the theoretical rise in pressure on the ramp is somewhat slower than the data (see remarks in Sec. VI).

Short Ramp Solutions

Figure 11 shows an infinite ramp solution and the corresponding family of short ramp solutions computed for the same solution upstream of the corner. These results were obtained by decreasing M_∞' below the infinite ramp value (corresponding to $\alpha = 36.96$ degrees) in suitable increments, resulting in larger values of α and smaller values of L_f/δ_0. The family of solutions represents the combination of ramp lengths and angles required to produce the same extent of separation upstream of the corner. By repeating these solutions for other values of $0 < H_c/H_s \leq 1$ at the same upstream Mach number and same value of n, a complete matrix of solutions is obtained with α and L_f/δ_0 as parameters. Typical results for the pressure at the trailing edge of the ramp (for infinite ramp solutions this pressure is taken to be the pressure at the critical point) from such a matrix is shown in Fig. 12 for $M_\infty = 6$ and $N = 8.7$ ($n = 13.6$).

Intersecting the dash-dot curves of constant H_c/H_s are curves of constant L_f/δ_0 which display some interesting characteristics. For L_f/δ_0 greater than about 1.7 a maximum in trailing edge pressure occurs at some critical angle§ α,

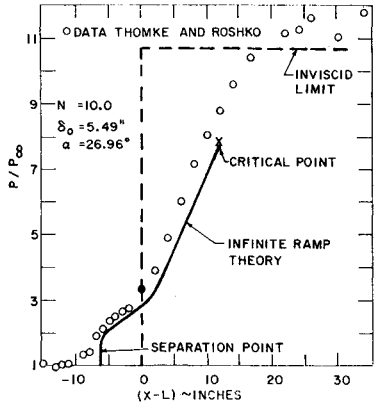

Fig. 9 Comparison of experimental and theoretical pressure distributions, $M = 5$, $Re = 0.96 \times 10^6$/in.

§ At present we can only give an upper bound for the critical α. This bound is defined by the infinite ramp solutions (solid curve) in Fig. 12. Complete solutions downstream of the critical point would have to be obtained to find precise values of the critical α.

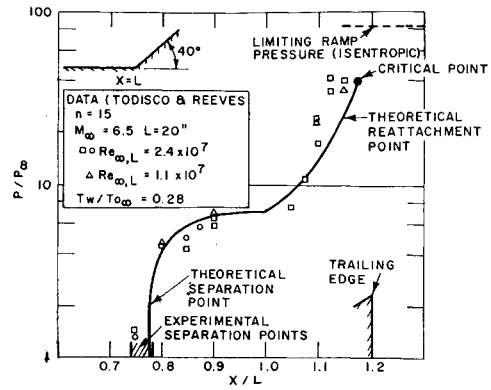

Fig. 10 Comparison of experimental and theoretical pressure distributions; cold wall, $M = 6.5$.

which depends on the value of L_f/δ_0. As α is increased above the critical value the pressure at the trailing edge decreases quite rapidly with angle as the reattachment point moves toward the trailing edge. For $L_f/\delta_0 < 1.7$ the pressure at the trailing edge increases steadily with increasing α. For large α all curves for constant L_f/δ_0 appear to approach a limiting pressure ratio, which is somewhat higher than the plateau pressure. For $L_f/\delta_0 = 1$ this limit is roughly 1.4 times the plateau pressure, whereas for $L_f/\delta_0 = 10$ the limit is almost twice the plateau pressure. Figure 12 shows that the incipient separation ramp angle is insensitive to ramp length as long as $L_f/\delta_0 > 1$.

Figure 13 shows some comparisons of the theory with experimental data obtained by Sterrett and Emery,[20] which demonstrates the strong influence of L_f/δ_0 on pressure recovery and extent of separation. The two sets of experimental pressure distributions in this figure were obtained by increasing the plate length preceeding the 34° ramp from 11 to 19 in. This produced a corresponding increase in δ_0 from 0.24 in. to 0.37 in. and a decrease in L_f/δ_0 from about 6.2 to 4.0. For $M_\infty = 5.8$, $\alpha = 34°$ and $n = 13.6$, it was found that $L_f/\delta_0 = 6.2$ resulted in an infinite ramp solution while $L_f/\delta_0 = 4.0$ produced a short ramp solution. Both theory and experiment indicate a longer separation distance upstream of the corner and a much slower rate of pressure recovery on the ramp for $L = 19$ in. The increase in δ_0 in this case caused nearly a 50% decrease in pressures on the ramp.

Further evidence of infinite ramp and short ramp behavior is evident in the experiments by Whitehead and Keyes[22] who measured pressure distributions on flaps attached to the trailing edge of a 70° delta wing planform at Mach 6. The

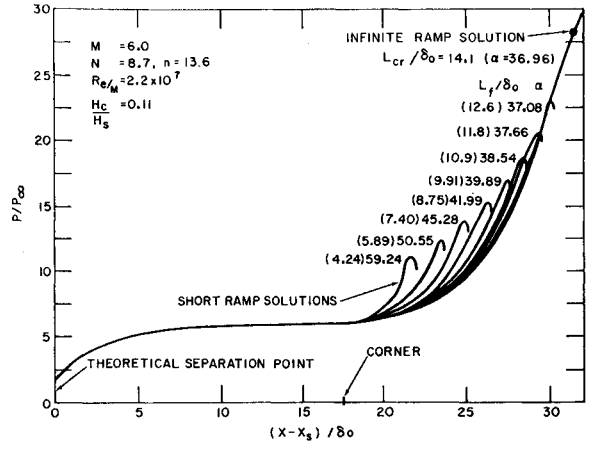

Fig. 11 Family of short ramp pressure distributions for same separation length, L_s/δ_0.

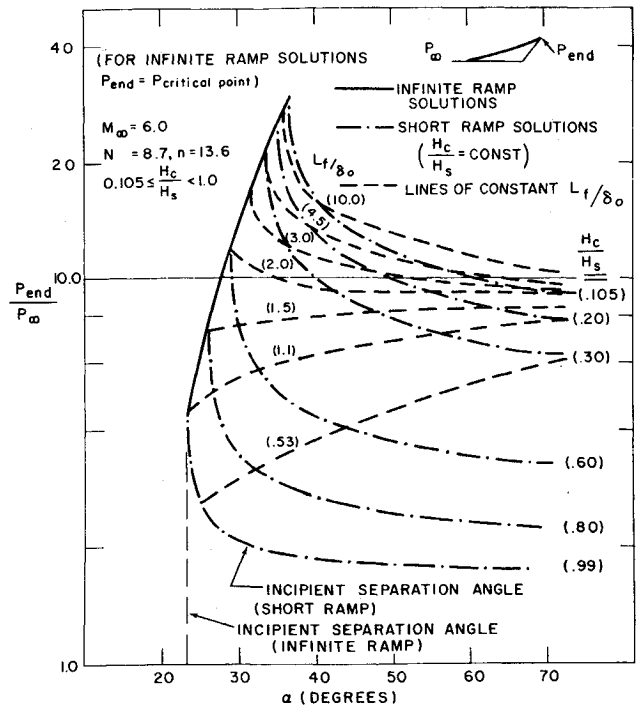

Fig. 12 Effect of ramp length and angle on peak pressure (or pressure at critical point for infinite ramp solutions).

experiment considered for comparison was performed with a 40° flap (ramp) angle, with the delta wing at zero angle of attack. When the boundary layer was tripped all along the leading edge, oil flow patterns over the wing showed that streamlines were everywhere parallel to the centerline and that a fairly regular but curved separation line was formed which varied from about 7 cm ahead of the hingeline at the centerline of the wing to about 2.3 cm ahead of the hingeline at full span. Calculations for this case were performed using a strip method. Since Whitehead and Keyes did not measure δ_0 and N across the wing, these were either scaled or taken directly from Sterrett and Emery,[20] who performed flat plate-ramp experiments in the same tunnel at the same Reynolds number and Mach number. This resulted in $N = 8.7$ all across the wing, and δ_0 equal to 0.65 cm, 0.49 cm, 0.34 cm and 0.18 cm at $y'/b = 0$, 0.2. 0.4 and 0.7, respectively.

Theoretical pressure distributions for a 37° flap on a delta wing are shown in Fig. 14 and can be compared with the experimental distributions measured by Whitehead and Keyes for a 40° flap. (Because the presently available range of profile functions only extends down to $H/H_s = 0.1$, the maximum ramp angle at $M_\infty = 6$ that can be solved as an infinite ramp solution is 37°. Ramp angles larger than 37° can be treated, however, if L_f/δ_0 falls into the range of short ramp solutions. One such short ramp solution was possible for the 40° flap along the centerline of the wing, and is shown in Fig. 14 with the experimental data). In the theoretical results for the 37° ramp the two inboard solutions are short ramp solutions while at the two outboard stations δ_0 was reduced sufficiently for the critical point to be located on the ramp. For the infinite ramp solutions at the two outboard stations the static pressure was extrapolated downstream of the critical point to the tangent wedge pressure for purposes of comparison with the data. The extrapolation was performed using the pressure gradient calculated at the critical point. Both theory and experiment show that the pressure recovery is much more rapid at the outboard stations of the wing. The pressure on the flap is lowest along the centerline, with reattachment occurring high up on the flap. By contrast, Fig. 5 of Ref. 22 shows the spanwise pressure distribution just reversed from

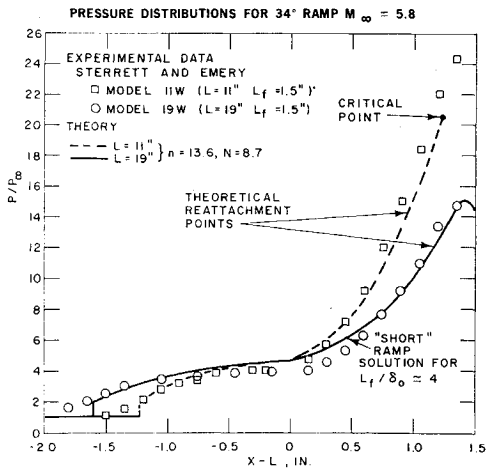

Fig. 13 Comparison of experimental and theoretical pressure distributions for infinite and short ramp solutions.

that shown in Fig. 14 as a result of not tripping the boundary layer. In this case the variation of transition distance with span caused an extremely complex transitional separation pattern with strong crossflows.

The variation of the separation length L_s with span (Fig. 14) agrees quite well with the separation point location indicated in Whitehead and Keyes' surface oil flow photographs for tripped boundary layers except very near full span where bleed from the recirculation region around the ramp was probably important.

Because of the short ramp behavior along the centerline of both configurations, the theoretical peak pressure at the trailing edge of the 37° flap exceeds the theoretical peak pressure on the 40° flap by about 25%.

V. Separated Flow on Ramps with Finite Span

If the aspect ratio of a ramp (S/L_f) is decreased to values smaller than about unity, complicated three-dimensional flows are produced not only in the recirculation region but in the separated and reattaching shear layer as well. In this situation part of the reattaching shear layer spills around the sides of the ramp.

For S/L_f roughly of order one or larger, however, depending on L_f/δ_0 and α, a semiempirical correction of the two-dimensional theory is proposed for calculating the extent of

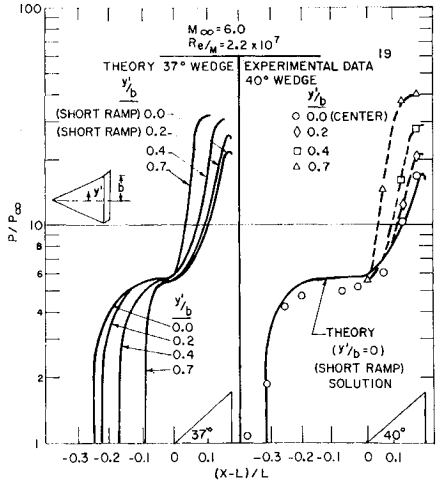

Fig. 14 Pressure distributions at various span locations for 37° and 40° ramps attached to the trailing edge of a delta wing.

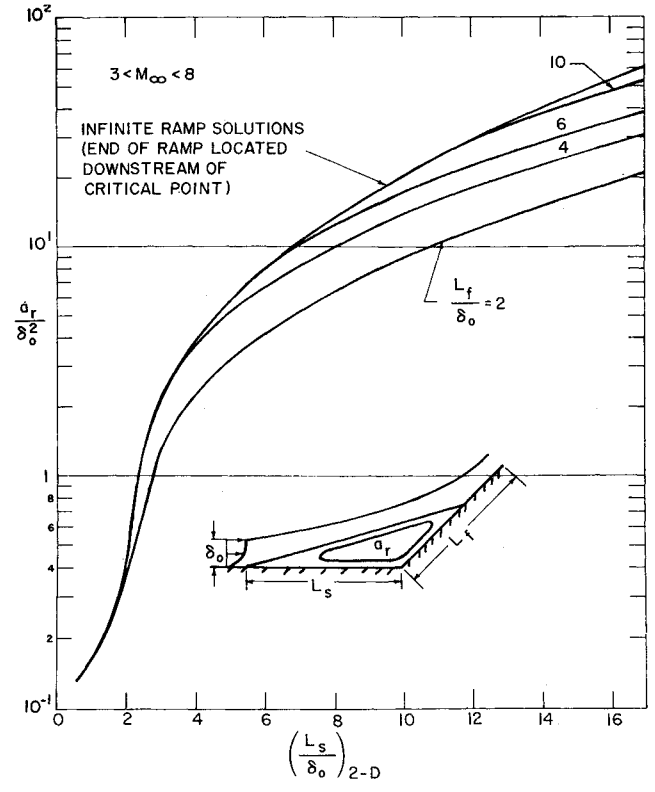

Fig. 15 Cross-sectional area of recirculation region as a function of separation length.

separation and pressure distribution along the center line of the ramp. Here we assume that for aspect ratios not too small the separated and reattaching flow above the dividing streamline remains in the same plane (or strip) normal to the surface but that a fraction of the low momentum flow in the recirculation region is bled around the edges of the ramp. It is further assumed that the reduction in cross-sectional area of the recirculation region is proportional to the mass flow bled from the recirculation region. Figure 15 shows the variation of the properly normalized cross-sectional area of the recirculation region with length of separation calculated using the present two-dimensional theory for infinite span. The curves are insensitive to variations in both Mach number and the profile parameter N upstream of separation.

Since the ratio of lateral mass bleed to the mass flow inside the recirculation region scales as $a_r/\delta_0 S$, or as $(a_r/\delta_0^2)(\delta_0/S)$, the ratio of separation lengths $(L_s/\delta_0)/(L_s/\delta_0)_{2-D}$ should scale with this "bleed parameter." Table 2 shows this dependence calculated from the experiments of Pate,[23] which were performed at Mach 3 for $\alpha = 30°$. Also, some unpublished AEDC data for $(a_r/\delta_0^2)(\delta_0/S) \simeq 6$ ($M_\infty = 8$, $\alpha = 40°$) have given quite good agreement with the theoretical pressure distributions if $(L_s/\delta_0)/(L_s/\delta_0)_{2-D} \simeq 0.35$. Table 2 summarizes these results.

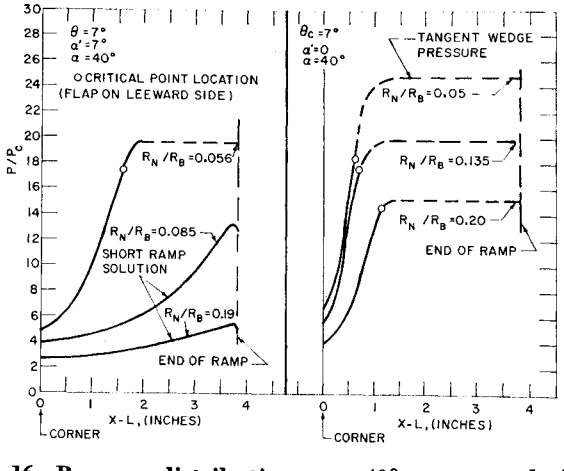

Fig. 16 Pressure distributions on a 40° ramp attached to a 7° blunted cone at 0° and 7° angle of attack.

Since all lengths in the separated flow interaction scale with the initial boundary layer thickness δ_0, a given two-dimensional interaction calculation can be used for finite span by simply normalizing all lengths in the streamwise direction by δ_0' for finite span, where $\delta_0'/\delta_0 = (L_s/\delta_0)/(L_s/\delta_0)_{2-D}$. The net result of these predictions for moderate span is that lateral flow out of the recirculation region promotes shorter separation and reattachment lengths and larger ramp pressures than in pure two-dimensional flow.

In order to demonstrate the influence of all the parameters considered thus far on ramp effectiveness, pressure distributions for separated flow past a 40° ramp, with $L_f = 3.8$ in. and $S = 3.5$ in., mounted at the trailing edge of a 7° half-angle cone were calculated. The cone base diameter was 8 inches. Two angles of attack were considered, $\alpha' = 0$ and 7 degrees, with the flap on the leeward side of the cone. Nose bluntness ratios, R_N/R_B, between 0 and 0.2 were also considered. All results were obtained for a freestream Mach number of 8.

Table 3 shows the local quantities calculated upstream of separation for each flow condition.

All local properties at the edge of the boundary layer upstream of separation were scaled using turbulent boundary layer swallowing estimates to account for variations in nose bluntness. The boundary-layer thickness was computed assuming turbulent flow from the nose. For $\alpha' = 7°$, δ_0 was calculated using Rainbird's[24] data for turbulent boundary-layer thickness on yawed cones at $M_\infty = 4.25$. Adjusting from a relative incidence of $\alpha'/\theta_c = 1.25$ used by Rainbird to the value of 1 here resulted in a ratio of boundary-layer thicknesses (δ_0 on leeward side for $\alpha' = 7$ degrees to δ_0 for $\alpha' = 0°$) about 2.5. The adjusted value of δ_0' to account for mass bleed from the recirculation region around the ramp is shown in Table 2 along with the compressible profile power law N, which was also estimated using Rainbird's profile data for $\alpha' = 7°$.

Pressure distributions on the ramp starting at the hinge line are shown in Fig. 16 for three bluntness ratios at each angle of attack. Here the ramp pressures are normalized by the local cone pressure ahead of separation. In the case of the infinite ramp solutions the pressure was extrapolated to the local tangent wedge pressure using the pressure gradient calculated at the critical point. Short ramp solutions, with considerably larger separated regions and much lower ramp pressures were found for the two largest bluntness ratios at $\alpha' = 7°$. These results show that the force on a leeward flap is much more sensitive to variations in nose bluntness than at zero angle of attack, with a sharp reduction in force for $\alpha' = 7°$ occurring at about $R_N/R_B = 0.06$.

VI. Concluding Remarks

Judging by these comparisons with experimental static pressure distributions, which have been made over a fairly wide range of ramp angles and flow conditions, the assumption that lateral pressure gradients are unimportant in the

Table 2 Effect of finite span on separation length

$(a_r/\delta_0^2)(\delta_0/S)$	0	0.2	0.61	6
$L_s/\delta_0/(L_s/\delta_0)_{2-D}$	1	0.91	0.47	$\simeq$0.35

subcritical flow region between the separation point and critical point appears to be borne out in most cases. Evidently, as long as the strong lateral pressure gradients that have been observed near reattachment are confined to the supercritical part of the compression downstream of the critical point the moment integral formulation can be expected to yield reliable predictions, at least up to about $M_\infty = 8$. In virtually all experimental comparisons made thus far, however, the measured static pressure along the surface rises somewhat more rapidly than the theoretical predictions downstream of the corner. This, of course, would be expected since p is computed along the edge of the layer and $\partial p/\partial y < 0$ for a concave flow.

These comparisons with experiments also seem to lend support to the wakelike model of the subcritical (separated) flow, with the stress profiles computed as though they were in local equilibrium with the wake-like velocity profiles (but not necessarily in equilibrium with the pressure gradient). This procedure for calculating the turbulent stress, which is equivalent to assuming that stress profiles are determined by the local value of Clauser's G function for attached incompressible flows, can be shown to produce peak stresses about 15–20% lower than the stress measurements of Bradshaw and Ferriss[25] in a strongly perturbed incompressible boundary layer as it passed from equilibrium in an adverse gradient to eventual equilibrium in zero pressure gradient. This stress lag is also consistent with the slightly slower pressure rise on the ramp predicted by the theory if the stress and velocity profiles are nearly in local equilibrium at the corner. An alternate series of calculations, assuming that K_θ remains frozen, i.e. $K_\theta = (K_\theta)_c$, between the corner and critical point could be used to approximate the effect of stress lag on the rate of pressure rise at reattachment.

Figure 17 shows a comparison of the interaction theory and some measurements of δ^* and H in the reattachment region of an incident shock wave-turbulent boundary-layer interaction at Mach 2.5. The experiments were performed by Green[26] for an over-all pressure ratio of about 3 (labeled a $9\frac{1}{2}°$ shock in Green's paper). Since the precise site of shock impingement with the layer was not determined by Green, the comparison was performed by setting the theoretical H and δ^* computed for this interaction equal to the respective experimental values at the first reported station (x = 23.5 in. in Green). This first point, which was located downstream of impingement, is given the notation x_0, and the displacement thickness and boundary-layer thickness at this point are $\delta_0{}^*$ and δ_0 in Fig. 17.

The distributions of H and δ^* downstream of this point, through reattachment, to the critical point are in excellent agreement with the experiments. Thus, it appears that even in the region of attached flow between reattachment and the critical point, which seldom exceeds 4 local boundary-layer thicknesses in length, the assumption of a wake-like flow with zero skin friction leads to quite reliable results. The wake-like flow assumption may be poorer for short ramps, however, because of rapid growth of the wall stress in the trailing edge expansion.

Table 3 Flow conditions computed upstream of separation for blunted 7° cone at $M_\infty = 8$

α' (deg)	R_N/R_B (per-cent)	$Re_L \times 10^{-6}$	M_{e_1}	δ_0 (in.)	(δ_0'/δ_0)	(L_{cr}/δ_0')	L_f/δ_0'	N
7	1.42	9.28	7.8	0.605	0.35	1.85		3.4
7	5.60	4.26	6.0	0.716	0.35	6.63		3.4
7	8.50	2.05	5.0	0.822	0.35		13.2	3.4
7	19.0	1.15	3.85	0.915	0.35		11.9	3.4
0	5.0	14.0	6.8	0.226	0.96	2.8		9
0	13.5	8.02	6.0	0.266	0.78	3.5		9
0	20.0	3.71	5.0	0.274	0.35	12.0		9

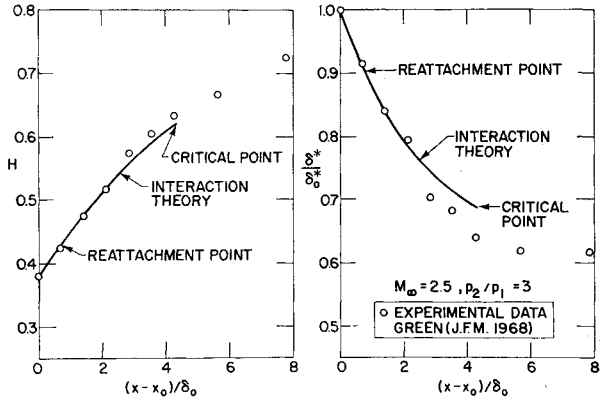

Fig. 17 H and δ^* variations downstream of shock wave-turbulent boundary-layer interaction.

It is apparent, at least for the case shown in Fig. 17, that effects of stress lag during reattachment on integral properties of the mean flow are generally insignificant upstream of the critical point. Whether this effect is important farther downstream in the supercritical relaxation to a new zero pressure gradient, equilibrium layer is not clear at present.

Although the present theory appears to predict length scales and pressure distributions for moderately cold walls, a theory capable of predicting heating rates in turbulent interactions must await inclusion of the energy equation. The wake-like approximation should be valid for the separated heat flux profiles as well. However, for infinite ramps the region of peak heating[6] apparently lies downstream of the critical point where a satisfactory interaction theory, which includes both the wall and wake layers, has yet to be developed even for adiabatic flows.

References

[1] Green, J. E., "Two-Dimensional Turbulent Reattachment as a Boundary Layer Problem," *Proceedings of the AGARD Specialists' Meeting on Separated Flows*, No. 4, May 1966, pp. 393–427.

[2] Alber, I. E. and L. Lees, "Integral Theory for Supersonic Turbulent Base Flows," *AIAA Journal*, Vol. 6, No. 7, July 1968, pp. 1343–1351.

[3] Reeves, B. L., "Turbulent Mixing in Supersonic Flow Past Slender Bodies with Large Blowing," *Proceedings of the AGARD Specialists Meeting on Separated Flows*, No. 4, May 1966, pp.303–324.

[4] Lees, L. and Chapkis, R. L., "Surface Mass Injection at Supersonic and Hypersonic Speeds as a Problem in Turbulent Mixing," *AIAA Journal*, Vol. 7, No. 4, April 1969, pp. 671–680.

[5] Fernandez, F. L. and Lees, L., "Effect of Finite Plate Length on Supersonic Turbulent Boundary Layers with Large Distributed Surface Injection," *AIAA Journal*, Vol. 8, No. 7, July 1970, pp. 1256–1263.

[6] Todisco, A. and Reeves, B. L., "Turbulent Boundary Layer Separation and Reattachment at Supersonic and Hypersonic Speeds," *Proceedings of Symposium on Viscous Interaction Phenomena in Supersonic and Hypersonic Flow*, 1969, University of Dayton Press, pp. 139–179.

[7] Crocco, L. and Lees, L., "A Mixing Theory for the Interaction Between Dissipative Flows and Nearly Isentropic Streams," *Journal of the Aerospace Sciences*, Vol. 19, 1952, pp. 649–676.

[8] Needham, D. A. and Stollery, J. L., "Boundary Layer Separation in Hypersonic Flow," AIAA Paper 66-455, Los Angeles, Calif., 1966.

[9] Zukoski, E. E., "Turbulent Boundary-Layer Separation in Front of a Forward-Facing Step," *AIAA Journal*, Vol. 5, No. 10, Oct. 1967, pp. 1746–1753.

[10] Crocco, L., "Considerations on the Shock-Boundary Layer Interaction," *Proceedings of the Conference on High-Speed Aeronautics*, Polytechnic Institute of Brooklyn, 1955, pp. 75–112.

[11] Seddon, J., "The Flow Produced by Interaction of a Turbulent Boundary Layer with a Normal Shock Wave of Strength Sufficient to Cause Separation," British R and M 3502, March 1960.

[12] Coles, D., "The Law of the Wake in the Turbulent Boundary Layer," *Journal of Fluid Mechanics*, Vol. 1, 1956, pp. 191–226.

[13] Clauser, F. H., "Turbulent Boundary Layers in Adverse Pressure Gradients," *Journal of the Aeronautical Sciences*, Vol. 21, No. 2, 1954, pp. 91–108.

[14] Clauser, F. H., "The Turbulent Boundary Layer," *Advances in Applied Mechanics*, Vol. IV, Academic Press, New York, 1956, pp. 1–51.

[15] Stratford, B. S., "An Experimental Flow with Zero Skin Friction Throughout Its Region of Pressure Rise," *Journal of Fluid Mechanics*, Vol. 5, 1959, pp. 17–35.

[16] Bradshaw, P. and Galea, P., "Step Induced Separation of a Turbulent Boundary Layer," *Journal of Fluid Mechanics*, Vol. 27, 1967, pp. 111–130.

[17] Mellor, G. L. and Gibson, D. M., "Equilibrium Turbulent Boundary Layers," *Journal of Fluid Mechanics*, Vol. 24, 1966, pp. 225–253.

[18] Lees, L. and Reeves, B. L., "Supersonic Separated and Reattaching Laminar Flows: I. General Theory and Application to Adiabatic Boundary Layer-Shock Wave Interactions," *AIAA Journal*, Vol. 2, No. 11, Nov. 1964, pp. 1907–1920.

[19] Thomke, G. J. and Roshko, A., "Incipient Separation of a Turbulent Boundary Layer at High Reynolds Number in Two-Dimensional Supersonic Flow over a Compression Corner," Rept. 59819, 1969, Douglas Aircraft; also *Proceedings of Symposium on Viscous Interaction Phenomena in Supersonic and Hypersonic Flow*, May 1969, University of Dayton Press, pp. 109–138.

[20] Sterrett, J. R. and Emery, J. C., "Experimental Separation Studies for Two-Dimensional Wedges and Curved Surfaces at Mach numbers of 4.8 to 6.2," TND-1014, 1962, NASA.

[21] Ko, D. R. S. and Kubota, T., "Supersonic Laminar Boundary Layer along a Two-Dimensional Adiabatic Curved Ramp," *AIAA Journal*, Vol. 7, No. 2, Feb. 1969, pp. 298–304.

[22] Whitehead, A. H. and Keyes, J. W., "Flow Phenomena and Separation over Delta Wings with Trailing Edge Flaps at Mach 6," *AIAA Journal*, Vol. 6, No. 12, Dec. 1968, pp. 2380–2387.

[23] Pate, S. R., "Investigation of Flow Separation on a Two-Dimensional Flat Plate Having a Variable-Span Trailing Edge Flap at $M = 3$ and 5," AEDC-TDR-64-14, March 1964, Arnold Engineering Development Center, Tenn.

[24] Rainbird, W. J., "Turbulent Boundary Layer Growth and Separation on a Yawed Cone," *AIAA Journal*, Vol. 6, No. 12, Dec. 1968, pp. 2410–2416.

[25] Bradshaw, P. and Ferriss, D. H., "The Response of a Retarded Equilibrium Turbulent Boundary Layer to the Sudden Removal of Pressure Gradient," British ARC 26758, NPL Aero Rept. 1145, March 1965.

[26] Green, J. E., "The Prediction of Turbulent Boundary Layer Development in Compressible Flow," *Journal of Fluid Mechanics*, Vol. 31, 1968, pp. 753–778; also private communication, July 1970.

[27] Bradshaw, P., "The Turbulence Structure of Equilibrium Boundary Layers," *Journal of Fluid Mechanics*, Vol. 29, 1967, pp. 625–645.

[28] Liepmann, H. W. and Laufer, J., "Investigations of Free Turbulent Mixing," TN 1257, 1947, NACA.

[29] Lewis, J. E., private communication, 1970, TRW Systems Group Inc., Redondo Beach, Calif.

APRIL 1971 AIAA JOURNAL VOL. 9, NO. 4

Aerodynamic Characteristics of a Slender Body Traveling in a Tube

THEODORE R. GOODMAN*
Oceanics Inc., Plainview, N. Y.

Incompressible inviscid slender-body theory is applied to determine the flow about a slender body of revolution traveling in a tube. Formulas for all the static and dynamic stability derivatives are derived for an arbitrary body of revolution in terms of its cross sectional area distribution. These formulas are specialized to an ellipsoid of revolution as an illustrative example and plots of the results are presented as a function of the ratio of the maximum cross-sectional area of the body to the area of the tube. For the body whose diameter is a large percent of the tube diameter, the stability derivatives become an order of magnitude greater than they are for the same body in free air. Furthermore, a statically unstable force of attraction to the wall caused by proximity to the wall is present which does not exist at all for the body in free air. The inherent aerodynamic instability of a body in free air without controls is thus increased by the presence of the tube walls, and the walls may be said to exert a large effect on the aerodynamic characteristics of the body.

Nomenclature

a = pivot point
C_L = L/qS_m = lift coefficient
C_M = $M/qS_m l$ = moment coefficient
C_p = pressure coefficient
$f(x)$ = see r_0
F = source strength
l = length of body
L = lift
M = pitching moment
q = $\frac{1}{2}\rho U^2$ = dynamic pressure
r = radial coordinate
r_0 = $\epsilon f(x)$ = body radius
R = tube radius
S_m = maximum cross-sectional area of body
S_0 = πr_0^2 = cross-sectional area of body
S_R = πR^2 = cross-sectional area of tube
t = time
U = freestream velocity
$\mathbf{V}$ = velocity vector
x = longitudinal coordinate
z_0 = heave displacement
α = S_0/S_R
α_m = S_m/S_R
β = potential due to heave displacement

Received April 30, 1969; revision received March 3, 1970. This work was supported by the Office of High Speed Ground Transportation of the United States Department of Commerce, now of the Department of Transportation.

* Vice President. Associate Fellow AIAA.